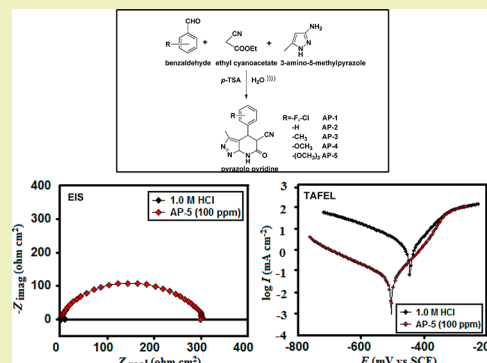


Ultrasound-Assisted Synthesis of Pyrazolo[3,4-*b*]pyridines as Potential Corrosion Inhibitors for Mild Steel in 1.0 M HClA. Dandia,<sup>†</sup> S. L. Gupta,<sup>†</sup> P. Singh,<sup>‡</sup> and M. A. Quraishi<sup>\*,‡</sup><sup>†</sup>Centre of Advance Studies, Department of Chemistry, University of Rajasthan, Jaipur-302004, India<sup>‡</sup>Department of Chemistry, Indian Institute of Technology, Banaras Hindu University, Varanasi-221005, India

**ABSTRACT:** Five synthesized pyrazolopyridine derivatives, such as 4-(2-chloro-6-flurpphenyl)-3-methyl-6-oxo-4,5,6,7-tetrahydro-2H-pyrazolo[3,4-*b*]-pyridine-5-carbonitrile (AP-1), 3-methyl-6-oxo-4,5,6,7-tetrahydro-2H-pyrazolo[3,4-*b*]pyridine-5-carbonitrile (AP-2), 3-methyl-6-oxo-4-(*p*-tolyl)-4,5,6,7-tetrahydro-2H-pyrazolo[3,4-*b*]pyridine-5-carbonitrile (AP-3), 4-(4-methoxyphenyl)-3-methyl-6-oxo-4,5,6,7-tetrahydro-2H-pyrazolo[3,4-*b*]pyridine-5-carbonitrile (AP-4), and 3-methyl-6-oxo-4-(3,4,5-trimethoxyphenyl)-4,5,6,7-tetrahydro-2H-pyrazolo[3,4-*b*]pyridine-5-carbonitrile (AP-5) have been synthesized using ultrasonic irradiation in aqueous medium using *p*-TSA as a catalyst, and their effect on corrosion of mild steel (MS) in 1.0 M HCl has been investigated using different experimental techniques like weight loss, electrochemical impedance spectroscopy (EIS), and potentiodynamic polarization techniques. The potentiodynamic polarization data indicated that the pyrazolo[3,4-*b*]pyridine derivatives behaved as a mixed type. The cathodic effect was more pronounced and AP-5 showed best inhibiting performance giving inhibition efficiency of 95.2% at 100 ppm. The adsorption of studied compounds obeyed the Langmuir adsorption isotherm.

**KEYWORDS:** Green synthesis, Mild steel, Acid solution, Weight loss, Electrochemical measurements



## INTRODUCTION

Corrosion causes enormous economic losses. Among the available methods of corrosion control, the use of corrosion inhibitors is one of the most effective and economic.<sup>1–5</sup>

Conventional methods used for synthesizing organic inhibitors are expensive and have long reaction times. Ultrasound-assisted synthesis has recently emerged as a powerful and green approach for synthesis of organic compounds. It offers several benefits compared with conventional techniques. In some cases, ultrasonic irradiation can increase reactivities by nearly a million-fold.<sup>6,7</sup> It does so through the process of acoustic cavitation: the formation, growth, and implosive collapse of bubbles in liquid. A large number of organic reactions can be carried out under ultrasonic irradiation with a short reaction time, high yield, and milder conditions.<sup>8–12</sup>

In recent years, being focused on green chemistry using environmentally benign reagents and conditions is one of the most fascinating developments in the synthesis of widely used organic compounds. Multicomponent domino reactions (MDRs),<sup>13–15</sup> particularly those performed in aqueous media, have become an increasingly useful tool for the synthesis of chemically and biologically important compounds because of their convergence, atom economy, and other suitable characteristics from the point of view of green chemistry.<sup>16–19</sup>

Pyrazolo[3,4-*b*]pyridine are a promising class of heterocyclic compounds. They exhibit a wide range of biological activities, such as antimicrobial, insecticidal, and anti-inflammatory

properties, and they are also used for the treatment of several diseases, including bipolar disorder, diabetes, dementia, Alzheimer's disease, schizophrenia, depression, and cancer.<sup>20–24</sup>

A literature survey revealed that a number of methods have been reported for the synthesis of pyrazolopyridines,<sup>25–28</sup> but all these methods suffered from drawbacks such as longer reaction time, lower yield, use of hazardous organic solvents and reagents, tedious workup procedures, and co-occurrence of several side reactions with less selectivity of the process. Thus, the search for new catalysts and methods is still of growing importance. A few of the pyrazolo[3,4-*b*]pyridine compounds have been investigated as corrosion inhibitors for metals and alloys in acid medium.<sup>29</sup>

In the present work, we wish to report the synthesis of pyrazolo[3,4-*b*]pyridine with a view to study their inhibitive action on corrosion of mild steel in 1.0 M HCl using weight loss, electrochemical impedance spectroscopy (EIS), and potentiodynamic polarization techniques. Survey and literature reveals that these compounds have been prepared for the first time by ultrasonicator technique.

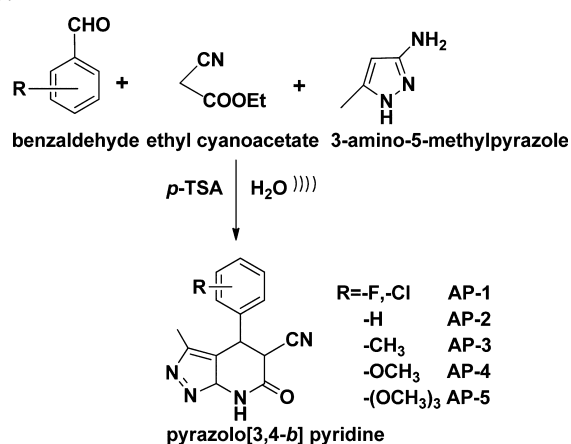
## EXPERIMENTAL SECTION

**Inhibitors.** The pyrazolo[3,4-*b*]pyridine derivatives were synthesized according to the given synthetic route in Scheme 1. Melting

Received: May 23, 2013

Revised: July 23, 2013

Published: July 29, 2013

Scheme 1. Synthetic Route for Preparation of Pyrazolo[3,4-*b*]pyridine Derivatives

points were recorded on a Toshniwal apparatus and are uncorrected. The purity of compounds was checked on thin layers of silica gel in various nonaqueous solvent systems, e.g., benzene:ethyl acetate (9:1) and n-hexane:ethyl acetate (7:3). IR spectra (KBr) were recorded on a Shimadzu FT IR-8400s spectrophotometer, and <sup>1</sup>HNMR and <sup>13</sup>CNMR spectra were recorded on a Bruker DRX-300 instrument at 300 and 75, respectively, in DMSO-*d*<sub>6</sub> relative to tetramethylsilane as an internal reference. The mass spectrum of the representative compound was recorded on a Waters Xevo Q-ToF spectrometer at 70 eV. Ultrasound irradiation was provided by an ultrasonic processor probe (Processor Sonopros PR-1000MP, OSCAR Ultrasonics with power input 230 V, 50 Hz, 4 Amps, and power variac 0–230 V and 3 Amps) operating at 20 kHz and 750W with 6 mm/12 mm tip diameter probes.

**General Procedure for Synthesis of 3-Methyl-6-oxo-4-phenyl-4,5,6,7-tetrahydro-2H-pyrazolo[3,4-*b*]pyridine-5-carbonitrile Derivatives (AP1–AP5).** A mixture of appropriate benzaldehyde (10 mmol), ethyl cyanoacetate (10 mmol), and 3-amino-5-methylpyrazole (10 mmol) and 10 mol % *p*-TSA in 20 mL water was introduced in a heavy walled pear-shaped two-necked flask with a nonstandard tapered outer joint. The flask was attached to a 12 mm tip diameter probe, and the reaction mixture was sonicated for the specified period at 50% power of the processor and in a 4 s pulse mode until a solid product separates out. Completion of the reaction was monitored by TLC using n-hexane:ethyl acetate (7:3) as the eluent. All the reactions were invariably complete in 50–70 min. Upon completion of the reaction, the solid product was filtered, washed with water, dried, and recrystallized from ethanol.

**Materials and Solutions.** The mild steel having the following composition (wt %) and balance Fe were used for weight loss studies: C 0.17%, Mn 0.46%, Si 0.026%, Cr 0.050%, P 0.012%, Cu 0.135%, Al 0.023%, and Ni 0.05%. For the weight loss study, mild steel coupons having dimensions of 2.5 cm × 2 cm × 0.025 cm were used. For the electrochemical study, coupons having dimensions of 8 cm × 1 cm × 0.025 cm with an exposed area of 1 cm<sup>2</sup>, and the rest covered by epoxy resin were used as the working electrode. The test solution of 1.0 M HCl was prepared by diluting analytical grade 37% HCl with double distilled water. The stock solution of inhibitors was prepared in 1.0 M HCl containing 1% acetone.

**Weight Loss Measurements.** Weight loss experiments were performed with abraded mild steel coupons by immersing it in 1.0 M HCl (100 mL) in the absence and presence of different pyrazolo[3,4-*b*]pyridine derivatives at different concentrations. After 3 h of immersion time, the coupons were taken out, washed, dried, and weighed accurately. The corrosion rate ( $C_R$ ), inhibition efficiency ( $\eta\%$ ), and surface coverage ( $\theta$ ) were determined by using following equations

$$C_R(\text{mm/y}) = \frac{87.6W}{atD} \quad (1)$$

$$\eta\% = \frac{C_R - {}^iC_R}{C_R} \times 100 \quad (2)$$

$$\theta = \frac{C_R - {}^iC_R}{C_R} \quad (3)$$

where  $W$  is the average weight loss of MS specimens,  $a$  is the total surface area of the MS specimen,  $t$  is the immersion time (3 h), and  $D$  is the density of MS (g cm<sup>-3</sup>). In eq 2,  $C_R$  and  ${}^iC_R$  are the corrosion rates of MS in the absence and presence of the inhibitors, respectively.

**Electrochemical Measurements.** The electrochemical experiments were performed by using three electrode cells connected to a potentiostat/galvanostat G300–45050 (Gamry Instruments, Inc., U.S.A.). An Echem Analyst 5.0 software package was used for data fitting. Mild steel was used as the working electrode with an exposed area of 1 cm<sup>2</sup>, a platinum electrode as an auxiliary electrode, and a saturated calomel electrode (SCE) as the reference electrode. All potentials reported were measured versus SCE. Tafel curves were obtained by changing the electrode potential automatically from –0.25 V to +0.25 V versus open corrosion potential at a scan rate of 1.0 mVs<sup>-1</sup>. Linear polarization resistance (LPR) experiments were done from –0.02 V to +0.02 V versus open corrosion potential at the scan rate of 0.125 mVs<sup>-1</sup>. EIS measurements were performed under potentiostatic conditions in a frequency range from 100 kHz to 0.01 Hz, with amplitude of 10 mV AC signal. The experiments were carried out after an immersion period of 30 min in 1.0 M HCl in the absence and presence of different concentrations of pyrazolo[3,4-*b*]pyridine derivatives.

## RESULTS AND DISCUSSION

Initially, the reaction between an equimolar ratio of benzaldehyde, ethyl cyanoacetate, and 3-amino-5-methylpyr-

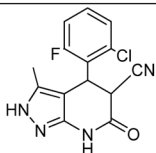
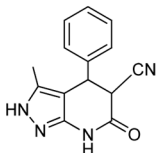
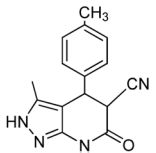
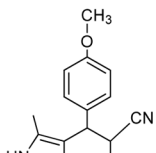
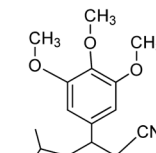
**Table 1.** Synthesis of Pyrazolo[3,4-*b*]pyridine-5-carbonitrile Derivatives (AP1–AP5)

compound	R	time (min)	yield (%) <sup>a</sup>	mp (°C)
AP-1	2-Cl-6-F	51	90	302–304
AP-2	4-H	62	86	294–296
AP-3	4-CH <sub>3</sub>	57	87	316–318
AP-4	4-OCH <sub>3</sub>	64	89	322–324
AP-5	3,4,5-OCH <sub>3</sub>	70	90	270–272

<sup>a</sup>Isolated yield.

azole was considered as a model reaction for optimization of reaction conditions. First, to find the specific effect of ultrasound on this reaction, the model reaction was carried out under conventional heating. There was no product formation in the absence of catalyst even after refluxing for 24 h, but when the model reaction was subjected to ultrasound irradiations, product AP-2 was obtained in moderate yield (31%) even after 160 min in absence of a catalyst. However, the results demonstrated the need of a catalyst because the yield of product was very low in the absence of catalyst. Therefore *p*-TSA was employed as catalyst for the said conversion. First, we checked the model reaction under conventional heating using *p*-TSA as a catalyst and found that the reaction took 11 h of heating with 69% yields. Thus, in order to develop a feasible approach, we used *p*-TSA as catalyst for the synthesis of pyrazolo[3,4-*b*]pyridine derivatives under ultrasound irradiations. All the compounds were synthesized in good to excellent yields in short reaction times (50–70 min) as compared to conventional heating. The significant increase in reaction rate under ultrasound irradiation could be ascribed to the simultaneous intensive enhancements of both heat and mass

Table 2. Molecular Structure and Analytical Data of Studied Inhibitors

Structure	Analytical data
 <p>4-(2-chloro-6-fluorophenyl)-3-methyl-6-oxo-4,5,6,7-tetrahydro-2H-pyrazolo[3,4-b]pyridine-5-carbonitrile (AP-1)</p>	<p>White powder (yield 90%); mp 302-304 °C; IR (KBr) <math>\text{cm}^{-1}</math>: 3612, 3344, 2248, 1716, 1536; <math>^1\text{H}</math> NMR (300 MHz, <math>\text{DMSO}-d_6</math>) <math>\delta</math>: 1.54 (s, 3H, <math>\text{CH}_3</math>), 4.74 (d, <math>^3J = 12.6</math> Hz, 1H, CH), 5.17 (d, <math>^3J = 12.6</math> Hz, 1H, CH), 7.18-7.54 (m, ArH, 3H), 10.97 (s, 1H, <math>\text{NH}_{\text{amid}}</math>), 12.11 (brs, 1H, <math>\text{NH}_{\text{pyrazole}}</math>) ppm. <math>^{13}\text{C}</math> NMR (75 MHz, <math>\text{DMSO}-d_6</math>) <math>\delta</math>: 9.95, 37.52, 44.24, 97.54, 116.62, 123.52, 125.84, 127.43, 133.71, 136.14, 147.32, 160.37, 162.78 ppm. MS ESI (m/z): 305 <math>[\text{M}+\text{H}]^+</math>.</p>
 <p>3-methyl-6-oxo-4,5,6,7-tetrahydro-2H-pyrazolo[3,4-b]pyridine-5-carbonitrile (AP-2)</p>	<p>White powder (yield 86%); mp 294-296 °C; IR (KBr) <math>\text{cm}^{-1}</math>: 3570, 3290, 2240, 1710, 1535; <math>^1\text{H}</math> NMR (300 MHz, <math>\text{DMSO}-d_6</math>) <math>\delta</math>: 1.49 (s, 3H, <math>\text{CH}_3</math>), 4.41 (d, <math>^3J = 12.0</math> Hz, 1H, CH), 4.65 (d, <math>^3J = 11.7</math> Hz, 1H, CH), 7.12-7.56 (m, 5H, ArH), 10.96 (s, 1H, <math>\text{NH}_{\text{amid}}</math>), 11.99 (brs, 1H, <math>\text{NH}_{\text{pyrazole}}</math>) ppm. <math>^{13}\text{C}</math> NMR (75 MHz, <math>\text{DMSO}-d_6</math>) <math>\delta</math>: 9.95, 36.82, 43.92, 101.05, 117.58, 127.95, 128.66, 130.29, 135.77, 137.76, 147.68, 163.61 ppm.; MS ESI (m/z): 253 <math>[\text{M}+\text{H}]^+</math>.</p>
 <p>3-methyl-6-oxo-4-(p-tolyl)-4,5,6,7-tetrahydro-2H-pyrazolo[3,4-b]pyridine-5-carbonitrile (AP-3)</p>	<p>White powder (yield 87%); mp 316-318 °C<sup>28</sup>; IR (KBr) <math>\text{cm}^{-1}</math>: 3575, 3315, 2250, 1710, 1542; <math>^1\text{H}</math> NMR (300 MHz, <math>\text{DMSO}-d_6</math>) <math>\delta</math>: 1.46 (s, 3H, <math>\text{CH}_3</math>), 2.31 (s, 3H, <math>\text{CH}_3</math>), 4.39 (d, <math>^3J = 11.7</math> Hz, 1H, CH), 4.66 (d, <math>^3J = 12</math> Hz, 1H, CH), 7.01-7.29 (m, 4H, ArH), 10.99 (s, 1H, <math>\text{NH}_{\text{amid}}</math>), 12.01 (brs, 1H, <math>\text{NH}_{\text{pyrazole}}</math>) ppm. <math>^{13}\text{C}</math> NMR (75 MHz, <math>\text{DMSO}-d_6</math>) <math>\delta</math>: 9.93, 21.18, 37.13, 44.04, 100.99, 117.70, 127.56, 128.40, 129.80, 135.81, 136.41, 137.51, 147.65, 163.59 ppm.; MS ESI (m/z): 267 <math>[\text{M}+\text{H}]^+</math>.</p>
 <p>4-(4-methoxyphenyl)-3-methyl-6-oxo-4,5,6,7-tetrahydro-2H-pyrazolo[3,4-b]pyridine-5-carbonitrile (AP-4)</p>	<p>White powder (yield 89%); mp 322-324 °C<sup>28</sup>; IR (KBr) <math>\text{cm}^{-1}</math>: 3566, 3274, 2238, 1694, 1530; <math>^1\text{H}</math> NMR (300 MHz, <math>\text{DMSO}-d_6</math>) <math>\delta</math>: 1.48 (s, 3H, <math>\text{CH}_3</math>), 3.77 (s, 3H, <math>\text{OCH}_3</math>), 4.38 (d, <math>^3J = 12.0</math> Hz, 1H, CH), 4.63 (d, <math>^3J = 12.0</math> Hz, 1H, CH), 6.87-7.32 (m, 4H, ArH), 10.93 (s, 1H, <math>\text{NH}_{\text{amid}}</math>), 11.96 (brs, 1H, <math>\text{NH}_{\text{pyrazole}}</math>) ppm. <math>^{13}\text{C}</math> NMR (75 MHz, <math>\text{DMSO}-d_6</math>) <math>\delta</math>: 9.92, 36.66, 44.16, 55.53, 101.24, 114.53, 117.73, 129.88, 131.24, 135.76, 147.62, 159.00, 163.64 ppm. MS ESI (m/z): 283 <math>[\text{M}+\text{H}]^+</math>.</p>
 <p>3-methyl-6-oxo-4-(3,4,5-trimethoxyphenyl)-4,5,6,7-tetrahydro-2H-pyrazolo[3,4-b]pyridine-5-carbonitrile (AP-5)</p>	<p>White powder (yield 90%); mp 270-272 °C; IR (KBr) <math>\text{cm}^{-1}</math>: 3562, 3268, 2256, 1714, 1528; <math>^1\text{H}</math> NMR (300 MHz, <math>\text{DMSO}-d_6</math>) <math>\delta</math>: 1.54 (s, 3H, <math>\text{CH}_3</math>), 3.69 (s, 3H, <math>\text{OCH}_3</math>), 3.73 (s, 6H, <math>\text{OCH}_3</math>), 4.41 (d, <math>^3J = 12</math> Hz, 1H, CH), 4.75 (d, <math>^3J = 11.7</math> Hz, 1H, CH), 6.48-6.86 (m, 2H, <math>\text{CH}_{\text{arom}}</math>), 10.94 (s, 1H, <math>\text{NH}_{\text{amid}}</math>), 11.97 (brs, 1H, <math>\text{NH}_{\text{pyrazole}}</math>) ppm. <math>^{13}\text{C}</math> NMR (75 MHz, <math>\text{DMSO}-d_6</math>) <math>\delta</math>: 9.64, 33.71, 41.64, 55.82, 56.05, 99.18, 100.68, 105.82, 117.42, 117.89, 129.36, 135.41, 147.94, 158.10, 160.65, 163.71 ppm. MS ESI (m/z): 343 <math>[\text{M}+\text{H}]^+</math>.</p>

transfer.<sup>20</sup> It is presumed that the efficiency using ultrasound irradiation is due to the cavitation phenomena. The chemical and physical effects of ultrasound arise from the cavitation collapse that produce extreme conditions locally and thus induce the formation of chemical species not easily attained under conventional conditions.<sup>30</sup> It is worthy to note that ultrasound with frequencies less than 50 kHz and the presence of solid *p*-TSA in the reaction mixture have resulted in an increase in the reaction rate as compared with the silent reaction because of the local rise in temperature and pressure

due to the cavitation of some bubbles next to the surface of the catalyst/reactants.<sup>31</sup>

On getting successful results, the general efficiency of this protocol was then studied for the synthesis of a variety of pyrazolo[3,4-*b*]pyridine-5-carbonitrile derivatives, and the results are summarized in Table 1. A series of aromatic aldehydes with both electron-donating and electron-withdrawing substituents were reacted with ethyl cyanoacetate and 3-amino-5-methylpyrazole under the optimized reaction conditions. As listed in Table 1, all reactions went smoothly

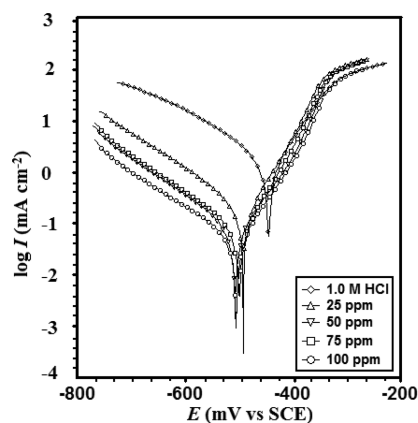


Figure 1. Tafel curves for mild steel in 1.0 M HCl without and with different concentrations of AP-5 at 308 K.

Table 3. Polarization Parameters for Mild Steel in 1.0 M HCl Solution Containing Different Concentrations of AP Compounds at 308 K

inhibitors	concentrations (ppm)	$I_{\text{corr}}$ ( $\mu\text{A cm}^{-2}$ )	$E_{\text{corr}}$ (mV/SCE)	$\beta_a$ (mV/dec)	$\beta_c$ (mV/dec)	$\eta\%$
blank	0.0	1390	-445	82	118	—
AP-1	25	445	-492	64	152	67.9
	50	262	-489	67	156	81.1
	75	210	-499	79	160	84.8
	100	131	-512	78	163	90.5
AP-2	25	269	-506	91	159	80.6
	50	179	-500	91	170	87.1
	75	156	-500	78	142	88.7
	100	123	-512	108	194	91.1
AP-3	25	223	-485	57	158	83.9
	50	158	-484	59	168	88.6
	75	127	-490	67	152	90.8
	100	82.8	-503	85	123	94.0
AP-4	25	208	-486	57	155	85.0
	50	129	-488	65	143	90.7
	75	115	-487	64	147	91.7
	100	76.5	-482	68	150	94.4
AP-5	25	191	-492	72	130	86.2
	50	104	-508	103	167	92.5
	75	79.3	-500	69	131	94.2
	100	65.5	-506	86	187	95.2

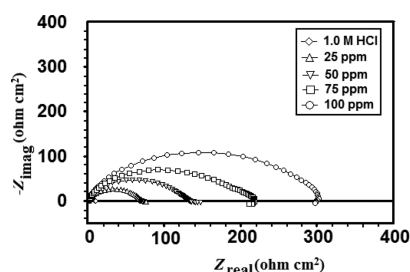


Figure 2. Nyquist plots for mild steel in 1.0 M HCl without and with different concentrations of AP-5 at 308 K.

under ultrasonic irradiation. The results indicated that the adopted procedure is equally feasible for both electron-rich and electron-deficient aldehydes. The reaction proceeded to completion rapidly, and products were obtained simply by

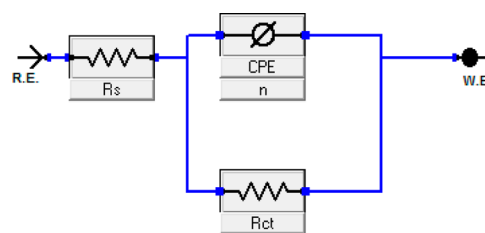


Figure 3. Equivalent circuit model used to fit EIS data.

filtration without involving any chromatographic purification. All the compounds were identified on the basis of IR,  $^1\text{H}$ ,  $^{13}\text{C}$ , and mass spectral studies, and data are listed in Table 2.

**Electrochemical Measurements.** *Potentiodynamic Polarization Measurements.* The polarization curves for mild steel in 1.0 M HCl in the absence and presence of pyrazolo[3,4-*b*]pyridine derivatives are shown in Figure 1, and electrochemical parameters obtained from these curves are listed in Table 3. It is shown that the addition of inhibitor causes a decrease in  $I_{\text{corr}}$  values. The maximum reduction of  $I_{\text{corr}}$  was obtained for (AP-5). It reduced  $I_{\text{corr}}$  from 445 to 65.5  $\mu\text{A cm}^{-2}$ , thereby giving an inhibition efficiency of 95.2% at 100 ppm. The values of  $\beta_c$  were changed more than  $\beta_a$ , indicating greater influence of the inhibitor molecules on the kinetics of hydrogen evolution.<sup>32</sup> The change in the  $E_{\text{corr}}$  value was not more than 85 mV with respect to the blank, which indicated that investigated pyrazolo[3,4-*b*]pyridines acts as a mixed type inhibitor.<sup>33,34</sup>

The inhibition efficiencies were calculated by  $I_{\text{corr}}$  values using following equation

$$\eta\% = \frac{I_{\text{corr}} - I_{\text{corr(inh)}}}{I_{\text{corr}}} \times 100 \quad (4)$$

where  $I_{\text{corr}}$  and  $I_{\text{corr(inh)}}$  are the corrosion current density in absence and presence of inhibitor, respectively, in 1.0 M HCl.

*Electrochemical Impedance Spectroscopy (EIS).* The results of the EIS measurements are presented in Figure 2 as Nyquist plots. The impedance parameters were calculated from these plots using equivalent circuit models shown in Figure 3 and listed in Table 4. The model consists of the solution resistance ( $R_s$ ), the charge-transfer resistance of the interfacial corrosion reaction ( $R_{\text{ct}}$ ), and the constant phase angle element (CPE).<sup>35</sup>

The inhibition efficiency is calculated using charge-transfer resistance ( $R_{\text{ct}}$ ) as follows,

$$\eta\% = \frac{R_{\text{ct(inh)}} - R_{\text{ct}}}{R_{\text{ct(inh)}}} \times 100 \quad (5)$$

where  $R_{\text{ct(inh)}}$  and  $R_{\text{ct}}$  are the values of charge-transfer resistance in the presence and absence of inhibitor in 1.0 M HCl, respectively.

It is shown that addition of pyrazolo[3,4-*b*]pyridine derivatives concentration increases the values of  $R_{\text{ct}}$  and decreases the values of  $C_{\text{dl}}$  on addition of inhibitors. The increase in  $R_{\text{ct}}$  values is attributed to an increase in resistance. The decrease in  $C_{\text{dl}}$  values is due to adsorption of inhibitor molecules on the mild steel surface. The values of double layer capacitance,  $C_{\text{dl}}$  were calculated from the following equation<sup>36</sup>

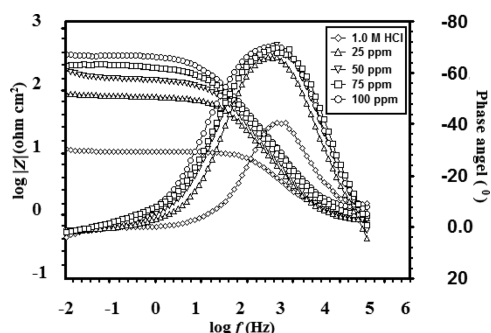
$$C_{\text{dl}} = Y_0(\omega_{\text{max}})^{n-1} \quad (6)$$

where  $Y_0$  is the CPE coefficient,  $n$  is the CPE exponent (phase shift), and  $\omega$  is the angular frequency.



**Table 4. Electrochemical Impedance Parameters and Corresponding Inhibition Efficiencies of Mild Steel in 1.0 M HCl in Absence and Presence of Different Concentrations of AP Compounds at 308 K**

inhibitors	concentrations (ppm)	$R_s$ ( $\Omega$ )	$R_{ct}$ ( $\Omega$ )	$n$	$Y_0$ ( $\mu\text{F cm}^{-2}$ )	$C_{dl}$	$\eta\%$
blank	0.0	1.02	9.0	0.82	250	106	—
AP-1	25	0.74	36.0	0.86	182	95	75.0
	50	0.76	49.4	0.84	155	71	81.7
	75	0.92	85.2	0.86	110	53	89.4
	100	0.74	119.2	0.86	106	49	92.4
AP-2	25	1.25	51.5	0.85	138	71	82.5
	50	0.88	84.3	0.84	142	61	89.3
	75	1.05	112.4	0.86	84	38	91.9
	100	1.10	186.8	0.86	73	32	95.1
AP-3	25	0.96	55.8	0.87	128	68	83.8
	50	1.19	91.2	0.83	141	56	90.1
	75	0.88	157.1	0.81	147	47	94.2
	100	0.76	242.4	0.83	84	28	96.2
AP-4	25	0.96	58.4	0.89	105	60	84.6
	50	0.81	117.4	0.84	103	41	92.3
	75	0.86	173.0	0.85	82	34	94.7
	100	1.04	256.7	0.88	53	25	96.4
AP-5	25	0.84	68.3	0.86	112	56	86.8
	50	0.79	129.3	0.85	95	40	93.0
	75	0.90	202.2	0.83	80	29	95.5
	100	1.19	294.3	0.85	67	25	96.9

**Figure 4.** Bode ( $\log f$  vs  $\log |Z|$ ) and phase angle ( $\log f$  vs  $\alpha$ ) plots of impedance spectra for mild steel in 1.0 M HCl in the presence of AP-5 at 308 K.

The thickness of this protective layer ( $d$ ) is correlated with  $C_{dl}$  by the following equation

$$C_{dl} = \frac{\epsilon \epsilon_0 A}{d} \quad (7)$$

where  $\epsilon$  is the dielectric constant,  $\epsilon_0$  is the permittivity of free space, and  $A$  is surface area of the electrode. Equation 6 suggests that  $C_{dl}$  is inversely proportional to the thickness of protective layer  $d$ .

The Bode plot and phase angle plot are plotted [ $\log |Z|$  vs  $\log f$ , and  $\alpha^\circ$  vs  $\log f$ ] are shown in Figure 4. An ideal capacitor behavior would result if a slope value attains  $-1$  and phase angle values attain  $-90^\circ$ . The deviation in presence of inhibitor AP-5 at 100 ppm slope is  $-0.79$ , and the phase angle approaching  $-70.85^\circ$  as compared with the blank slope is  $-0.53$  and phase angle value is  $-40.40^\circ$ . The deviation of bode and phase angle values from ideal values suggest the capacitive performance of the inhibited system.<sup>37</sup>

**Weight Loss Measurements.** *Effect of Inhibitor Concentration.* The effect of different concentration of inhibitors was studied by weight loss technique. The results are given in Table 5. It is seen that inhibition efficiency increase with increasing

**Table 5. Parameters Obtained from Weight Loss Measurements for Mild Steel in 1.0 M HCl Containing Different Concentrations of AP Compounds at 308 K**

inhibitors	concentrations (ppm)	corrosion rate (mm/y)	surface coverage ( $\theta$ )	$\eta\%$
blank	0.0	77.9	—	—
AP-1	25	18.92	0.75	75.7
	50	17.06	0.78	78.0
	75	14.09	0.81	81.9
	100	11.13	0.85	85.7
AP-2	25	14.28	0.81	81.6
	50	11.50	0.85	85.2
	75	9.27	0.88	88.0
	100	8.16	0.89	89.5
AP-3	25	12.80	0.83	83.5
	50	8.34	0.89	89.2
	75	6.30	0.91	91.9
	100	4.26	0.94	94.5
AP-4	25	11.31	0.85	85.4
	50	7.42	0.90	90.4
	75	4.82	0.93	93.8
	100	3.89	0.95	95.0
AP-5	25	10.57	0.86	86.4
	50	5.19	0.93	93.3
	75	4.63	0.94	94.0
	100	2.96	0.96	96.1

pyrazolo[3,4-*b*]pyridine concentrations and best inhibition efficiency obtained for AP-5 is 96.1% at 100 ppm concentration. This may be due to the adsorption of pyrazolo[3,4-*b*]pyridine molecules leading to the formation of a smooth layer on metal surface which prevents the contact of metal with the surrounding acidic environment and higher bonding ability of inhibitor on the mild steel surface is due to the higher number of lone pairs on heteroatom's and  $\pi$  orbital's.<sup>38,39</sup>

**Adsorption Isotherm.** The interaction between the pyrazolo[3,4-*b*]pyridine derivatives and metal surface can be interpreted

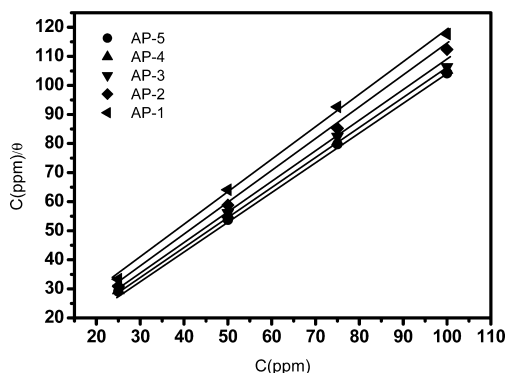


**Figure 5.** Langmuir isotherms for adsorption of AP compounds on mild steel surfaces in 1.0 M HCl.

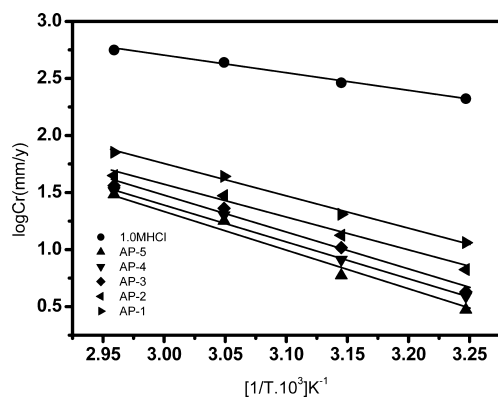


**Figure 6.** Arrhenius plots of  $\log C_R$  vs  $1000/T$  for mild steel in 1.0 M HCl in the absence and presence of AP compounds at optimum concentrations.

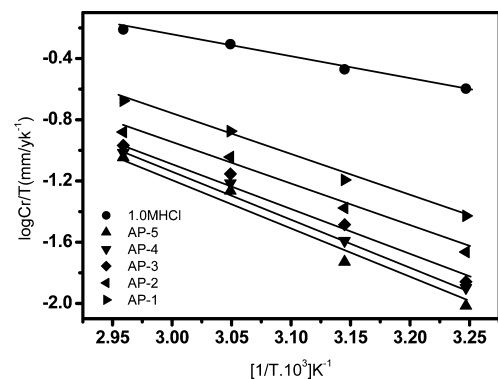


**Figure 7.** Arrhenius plots of  $\log C_R/T$  vs  $1000/T$  for mild steel in 1.0 M HCl in the absence and presence AP compounds at optimum concentration.

**Table 6. Activation Parameters for Mild Steel Dissolution in 1.0 M HCl in Absence and Presence of Optimum Concentration of Investigated AP Compounds**

inhibitors	$E_a$ (kJ mol <sup>-1</sup> )	$\Delta H_a$ (kJ mol <sup>-1</sup> )	$\Delta S_a$ (JK <sup>-1</sup> mol <sup>-1</sup> )
blank	29.10	26.42	-123.27
AP-1	54.0	51.32	-58.46
AP-2	56.33	53.64	-55.05
AP-3	62.75	60.07	-37.54
AP-4	63.11	60.43	-37.63
AP-5	70.02	67.34	-17.81

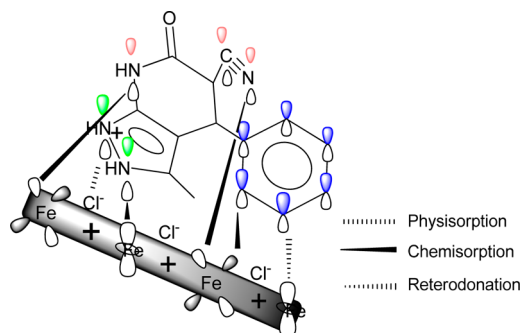


**Figure 8.** Pictorial representation of the mechanism of adsorption of AP compounds on the MS surface.

by the adsorption isotherm. The addition of different concentrations of pyrazolo[3,4-*b*]pyridine derivatives rapidly forms a protective layer on the metal surface through the metal–solution interface because the solid MS surface contains a fixed number of adsorption sites and each site holds one adsorbed species. The surface coverage,  $\theta$ , covered after adsorption, was calculated according to eq 3.

By fitting the degree of surface coverage ( $\theta$ ) to adsorption isotherms, including Frumkin, Temkin, and Langmuir isotherms, the best fit was obtained in the case of the Langmuir isotherm by plotting  $(C/\theta)$  vs  $C$ , which gives a straight line with a regression coefficient  $R^2$  value near to about one as shown in Figure 5. The equation is represented as

$$K_{\text{ads}} = \frac{\theta}{C(1 - \theta)} \quad (8)$$

The equation can be rearranged as

$$\frac{C_{\text{inh}}}{\theta} = \frac{1}{K_{\text{ads}}} + C_{\text{inh}} \quad (9)$$

where  $C_{\text{inh}}$  is the concentration of inhibitor, and  $\theta$  is surface area.

$K_{\text{ads}}$  is related to the standard free energy of adsorption  $\Delta G_{\text{ads}}$  by the following equation

$$\Delta G_{\text{ads}} = -RT \ln(55.5K_{\text{ads}}) \quad (10)$$

where  $R$  is the gas constant, and  $T$  is the absolute temperature. The value of 55.5 is the concentration of water in solution in mol L<sup>-1</sup>.

The calculated values of  $\Delta G_{\text{ads}}$  at optimum concentration and 308 K range from  $-39.2$  to  $-35.2$  kJ mol<sup>-1</sup> and indicate that the adsorption of the inhibitor molecules on the MS surface may involve both physical as well as chemical adsorption.<sup>40</sup>

**Effect of Temperature.** The temperature effect on the mild steel surface during increasing temperature from 308–338 K can be understood by thermodynamic activation parameters. With the increase in temperature, the inhibition efficiency decreases because of desorption of the adsorbed molecule on the metal surface, and metal comes in direct contact with the acidic medium. The activation energy can be calculated using following equation

$$\ln(C_R) = \frac{-E_a}{RT} + A \quad ([11])$$

where  $E_a$  is the activation energy for corrosion of MS in 1.0 M HCl,  $R$  is the gas constant,  $A$  is the Arrhenius pre-exponential

factor, and  $T$  is the absolute temperature. A plot of the corrosion rate  $\ln C_R$  vs  $1000/T$  gives a straight line as shown in Figure 6. The values of  $E_a$  in 1.0 M HCl in the absence and presence of pyrazolo[3,4-*b*]pyridine derivatives are determined from the slope by plotting the values obtained. The enthalpy and entropy of activation ( $\Delta H^*$  and  $\Delta S^*$ ) can be calculated by given equation

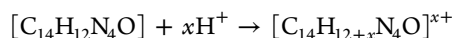
$$C_R = \frac{RT}{Nh} \exp\left(\frac{\Delta S^*}{R}\right) \exp\left(-\frac{\Delta H^*}{RT}\right) \quad (12)$$

where  $h$  is Planck's constant, and  $N$  is Avogadro's number.

A plot of  $\ln(C_R/T)$  against  $1000/T$  is shown in Figure 7, which gives straight lines with a slope of  $(-\Delta H^*/R)$  and an intercept of  $[(\ln(R/Nh)) + (\Delta S^*/R)]$  to which the values of  $\Delta H^*$  and  $\Delta S^*$  are calculated and are listed in Table 6.

The higher values of  $E_a$  and  $\Delta H^*$  indicate creation of an energy barrier for the corrosion reaction in the presence of the inhibitor.<sup>41,42</sup> The higher values of  $\Delta S^*$  for inhibited solutions might be the result of the adsorption of inhibitor molecules from the 1.0 M HCl solution, which could be regarded as a quasi-substitution process between the pyrazolo[3,4-*b*]pyridine molecules in the aqueous phase and water molecules on the mild steel surface.<sup>43,44</sup>

**Mechanism of Adsorption and Inhibition.** In a hydrochloric acid solution, the pyrazolo[3,4-*b*]pyridine derivatives exist either as neutral molecules or in protonated form.



Pyrazolo[3,4-*b*]pyridine derivatives may adsorb on the metal–acid solution interface in one or more of the following ways: (i) electrostatic interaction of protonated pyrazole derivative with already adsorbed chloride ions, (ii) donor–acceptor interactions between the p-electrons of the aromatic ring and the vacant d-orbital of surface iron atom,s and (iii) interaction between unshared electron pairs of hetero-atoms and the vacant d-orbital of surface iron atoms as shown in Figure 8. The following way of adsorption of pyrazolo[3,4-*b*]pyridine derivatives results in a smooth layer of adsorbed molecules on a metal surface, which forms a barrier between metal and the acidic solution that slows down the metal dissolution and protects the metal from a corrosive environment.<sup>45,46</sup>

## CONCLUSIONS

The results obtained for pyrazolo[3,4-*b*]pyridine derivatives showed that among the five pyrazolo[3,4-*b*]pyridine derivatives AP-5 is the best inhibitor and gives 96.1% inhibition efficiency at 100 ppm. The potentiodynamic polarization data indicated that the pyrazolo[3,4-*b*]pyridine derivatives were of a mixed type, but the cathodic effect was more pronounced. Electrochemical impedance spectroscopy data reveals a decrease in  $C_{dl}$  values that can result from a decrease in the local dielectric constant or an increase in the thickness of the electrical double layer. The adsorption of the inhibitor molecules on the mild steel surface was found to obey the Langmuir adsorption isotherm. All these data support the good inhibition tendency of pyrazolo[3,4-*b*]pyridine derivatives.

## AUTHOR INFORMATION

### Corresponding Author

\*E-mail: maquraishi@rediffmail.com, maquraishi.apc@itbhu.ac.in.

## Notes

The authors declare no competing financial interest.

## ACKNOWLEDGMENTS

Priyanka Singh is thankful to the University Grants Commission (UGC), New Delhi, for the Project (40-101/2011) SR Fellowship, and Anshu Dandia is thankful to the CSIR [02(0143)/13/EMR-II], New Delhi.

## REFERENCES

- (1) Tao, Z.; Zhang, S.; Li, W. Baorong Hou Corrosion inhibition of mild steel in acidic solution by some oxo-triazole derivatives. *Corros. Sci.* **2009**, *51*, 2588–2595.
- (2) Ashassi-Sorkhabi, H.; Shaabani, B.; Seifzadeh, D. Effect of some pyrimidinic Schiff bases on the corrosion of mild steel in hydrochloric acid solution. *Electrochim. Acta* **2005**, *50*, 3446–3452.
- (3) Li, X.; Deng, S.; Fu, H. Inhibition of the corrosion of steel in HCl, H<sub>2</sub>SO<sub>4</sub> solutions by bamboo leaf extract. *Corros. Sci.* **2012**, *62*, 163–175.
- (4) Hussin, M. H.; Kassim, M. J. The corrosion inhibition and adsorption behavior of Uncaria gambir extracts on mild steel in 1M HCl. *Mater. Chem. Phys.* **2011**, *125*, 461–468.
- (5) Oguzie, E. E. Evaluation of the inhibitive effect of some plant extracts on the acid corrosion of mild steel. *Corros. Sci.* **2008**, *50*, 2993–2998.
- (6) Nasir Baig, R. B.; Varma, R. S. Alternative energy input: Mechanochemical, microwave and ultrasound-assisted organic synthesis. *Chem. Soc. Rev.* **2012**, *41*, 1559–1584.
- (7) Dandia, A.; Singh, R.; Bhaskaran, S. Facile stereoselective synthesis of spiro[indole-oxiranes] by combination of phase transfer catalyst and ultrasound irradiation and their bioassay. *Ultrason. Sonochem.* **2011**, *18*, 1113–1117.
- (8) Joshi, R. S.; Mandhane, P. G.; Diwakar, S. D.; Gill, C. H. Ultrasound assisted green synthesis of bis(indol-3-yl)methanes catalyzed by 1-hexenesulphonic acid sodium salt. *Ultrason. Sonochem.* **2010**, *17*, 298–300.
- (9) Dandia, A.; Bhati, D. S.; Jain, A. K.; Sharma, G. N. Ultrasound promoted clay catalyzed efficient and one pot synthesis of substituted oxindoles. *Ultrason. Sonochem.* **2011**, *18*, 1143–1147.
- (10) Nabid, M. R.; Tabatabaei-Rezaei, S. J.; Ghahremanzadeh, R.; Bazgir, A. Ultrasound-assisted one-pot, three-component synthesis of 1*H*-pyrazolo[1,2-*b*]phthalazine-5,10-diones. *Ultrason. Sonochem.* **2010**, *17*, 159–161.
- (11) Li, J. T.; Liu, X. R.; Sun, M. X. Synthesis of glycoluril catalyzed by potassium hydroxide under ultrasound irradiation. *Ultrason. Sonochem.* **2010**, *17*, 55–57.
- (12) Li, J. T.; Yin, Y.; Sun, M. X. An efficient one-pot synthesis of 2,3-epoxyl-1,3-diaryl-1-propanone directly from acetophenones and aromatic aldehydes under ultrasound irradiation. *Ultrason. Sonochem.* **2010**, *17*, 363–366.
- (13) Ganem, B. Strategies for innovation in multicomponent reaction design. *Acc. Chem. Res.* **2009**, *42*, 463–472.
- (14) Dandia, A.; Jain, A. K.; Sharma, S. Indium triflate catalyzed one-pot multicomponent synthesis of spiro-hexahydropyrimidines explained by multiple covalent bond formation. *Tetrahedron Lett.* **2012**, *53*, 5270–5274.
- (15) Singh, M. S.; Chowdhury, S. Recent developments in solvent-free multicomponent reactions: a perfect synergy for eco-compatible organic synthesis. *RSC Adv.* **2012**, *2*, 4547–4592.
- (16) Li, C. J.; Chen, L. Organic chemistry in water. *Chem. Soc. Rev.* **2006**, *35*, 68–82.
- (17) Li, C. J. Organic reactions in aqueous media with a focus on carbon–carbon bond formations: A decade update. *Chem. Rev.* **2005**, *105*, 3095–3166.
- (18) Dandia, A.; Parewa, V.; Jain, A. K.; Rathore, K. S. Step-economic, efficient, ZnS nanoparticle-catalyzed synthesis of spirooxindole derivatives in aqueous medium via Knoevenagel condensation followed by Michael addition. *Green Chem.* **2011**, *13*, 2135.

- (19) Dandia, A.; Singh, R.; Bhaskaran, S.; Samant, S. D. Versatile three component procedure for combinatorial synthesis of biologically relevant scaffold spiro[indole-thiazolidinones] under aqueous conditions. *Green Chem.* **2011**, *13*, 1852.
- (20) Chavatte, P.; Yous, S.; Marot, C.; Baurin, N.; Lesieur, D. Three-dimensional quantitative structure–activity relationships of cyclooxygenase-2 (COX-2) inhibitors: A comparative molecular field analysis. *J. Med. Chem.* **2001**, *44*, 3223–3230.
- (21) Stika, C. S.; Gross, G. A.; Leguizamón, G.; Gerber, S.; Levy, R.; Mathur, A.; Bernhard, L. M.; Nelson, D. M.; Sadovsky, Y. A prospective randomized safety trial of celecoxib for treatment of preterm labor. *Am. J. Obstet. Gynecol.* **2002**, *187*, 653–660.
- (22) Dilger, K.; Herrlinger, C.; Peters, J.; Seyberth, H. W.; Schweer, H.; Klotz, U. Effects of celecoxib and diclofenac on blood pressure, renal function, and vasoactive prostanoids in young and elderly subjects. *J. Clin. Pharmacol.* **2002**, *42*, 985–694.
- (23) Fong, T. M.; Heymsfield, S. B. Cannabinoid-1 receptor inverse agonists: current understanding of mechanism of action and unanswered questions. *Int. J. Obs.* **2009**, *33*, 947–955.
- (24) Bristow, D. R.; Martin, I. L. Biochemical characterization of an isolated and functionally reconstituted  $\gamma$ -aminobutyric acid/benzodiazepine receptor. *J. Neurochem.* **1990**, *54*, 751–761.
- (25) Balamurugan, K.; Perumal, S.; Menéndez, J. C. New four-component reactions in water: a convergent approach to the metal-free synthesis of spiro[indoline/acenaphthylene-3,4'-pyrazolo[3,4-*b*]pyridine derivatives. *Tetrahedron* **2011**, *67*, 3201–3208.
- (26) Quiroga, J.; Portillo, S.; Pérez, A.; Gálvez, J.; Abonia, R.; Insuasty, B. An efficient synthesis of pyrazolo[3,4-*b*]pyridine-4-spiroindolinones by a three-component reaction of 5-aminopyrazoles, isatin, and cyclic  $\beta$ -diketones. *Tetrahedron Lett.* **2011**, *52*, 2664–2666.
- (27) Quiroga, J.; Trilleras, J.; Pantoja, D.; Abonia, R.; Insuasty, B.; Nogueras, M.; Cobo, J. Microwave-assisted synthesis of pyrazolo[3,4-*b*]pyridinespirocycloalkanediones by three-component reaction of 5-aminopyrazole derivatives, paraformaldehyde and cyclic  $\beta$ -diketones. *Tetrahedron Lett.* **2010**, *51*, 4717–4719.
- (28) Rahmati, A. Synthesis of 4-aryl-3-methyl-6-oxo-4,5,6,7-tetrahydro-2*H*-pyrazolo[3,4-*b*]pyridine-5-carbonitrile via a one-pot, three-component reaction. *Tetrahedron Lett.* **2010**, *51*, 2967–2970.
- (29) El-Mhammedi, M. A.; Chtaini, A. Investigation of the inhibitive effect of pyrazolo[3,4-*b*]pyridine on corrosion of stainless steel in 1 M HCl solutions. *Leonardo Electron. J. Pract. Technol.* **2007**, *11*, 37–46.
- (30) Mason, T. J. Ultrasound in synthetic organic chemistry. *Chem. Soc. Rev.* **1997**, *26*, 443–45.
- (31) Cravotto, G.; Gaudino, E. C.; Cintas, P. On the mechanochemical activation by ultrasound. *Chem. Soc. Rev.* **2013**, DOI: 10.1039/c2cs35456j.
- (32) Negma, N. A.; Kandile, N. G.; Aiada, I. A.; Mohammad, M. A. New eco-friendly cationic surfactants: Synthesis, characterization and applicability as corrosion inhibitors for carbon steel in 1 N HCl. *Colloids Surf., A* **2011**, *391*, 224–233.
- (33) Satapathy, A. K.; Gunasekaran, G.; Sahoo, S. C.; Amit, K.; Rodrigues, P. V. Corrosion inhibition by *Justicia gendarussa* plant extract in hydrochloric acid solution. *Corros. Sci.* **2009**, *51*, 2848–2856.
- (34) Khaled, K. F.; Amin, M. A. Corrosion monitoring of mild steel in sulphuric acid solutions in presence of some thiazole derivatives—Molecular dynamics, chemical and electrochemical studies. *Corros. Sci.* **2009**, *51*, 1964–1975.
- (35) Yadav, D. K.; Maiti, B.; Quraishi, M. A. Electrochemical and quantum chemical studies of 3,4-dihydropyrimidin-2(1*H*)-ones as corrosion inhibitors for mild steel in hydrochloric acid solution. *Corros. Sci.* **2010**, *52*, 3586–3598.
- (36) Shukla, S. K.; Quraishi, M. A. The effects of pharmaceutically active compound doxycycline on the corrosion of mild steel in hydrochloric acid solution. *Corros. Sci.* **2010**, *52*, 314–321.
- (37) Yadav, D. K.; Quraishi, M. A.; Maiti, B. Inhibition effect of some benzylidenes on mild steel in 1 M HCl: An experimental and theoretical correlation. *Corros. Sci.* **2012**, *55*, 254–266.
- (38) Deng, Q.; Shi, H. W.; Ding, N. N.; Chen, B. Q.; He, X. P.; Liu, G.; Tang, Y.; Long, Y. T.; Chen, G. R. Novel triazolyl bis-amino acid derivatives readily synthesized via click chemistry as potential corrosion inhibitors for mild steel in HCl. *Corros. Sci.* **2012**, *57*, 220–227.
- (39) Tao, Z.; Hea, W.; Wang, S.; Zhang, S.; Zhou, G. A study of differential polarization curves and thermodynamic properties for mild steel in acidic solution with nitrophenyltriazole derivative. *Corros. Sci.* **2012**, *60*, 205–213.
- (40) Ahamad, I.; Prasad, R.; Quraishi, M. A. Thermodynamic, electrochemical and quantum chemical investigation of some Schiff bases as corrosion inhibitors for mild steel in hydrochloric acid solutions. *Corros. Sci.* **2010**, *52*, 933–942.
- (41) Ahamad, I.; Prasad, R.; Quraishi, M. A. Inhibition of mild steel corrosion in acid solution by Pheniramine drug: Experimental and theoretical study. *Corros. Sci.* **2010**, *52*, 3033–3041.
- (42) Ahamad, I.; Quraishi, M. A. Bis (benzimidazol-2-yl) disulphide: An efficient water soluble inhibitor for corrosion of mild steel in acid media. *Corros. Sci.* **2009**, *51*, 2006–2013.
- (43) Singh, A. K.; Quraishi, M. A. Inhibitive effect of diethylcarbazine on the corrosion of mild steel in hydrochloric acid. *Corros. Sci.* **2010**, *52*, 1529–1535.
- (44) Ahamad, I.; Quraishi, M. A. Adsorption and inhibitive properties of some new Mannich bases of Isatin derivatives on corrosion of mild steel in acidic media. *Corros. Sci.* **2010**, *52*, 1472–1481.
- (45) Singh, A. K.; Quraishi, M. A. The effect of some bis-thiadiazole derivatives on the corrosion of mild steel in hydrochloric acid. *Corros. Sci.* **2010**, *52*, 1373–1385.
- (46) Yadav, D. K.; Quraishi, M. A. Application of some condensed uracils as corrosion inhibitors for mild steel: gravimetric, electrochemical, surface morphological, UV-visible, and theoretical investigations. *Ind. Eng. Chem. Res.* **2012**, *51*, 14966–14979.